

DTIC FILE COPY

4

Offaxis Radiance Studies for Infrared Sensors

AD-A210 790

Andrew J. Mazzella, Jr.
Steven A. Lacaire

RDP Inc.
Waltham Office Center
486 Totten Pond Road
Waltham, MA 02154

27 December 1988

Scientific Report No. 1


DTIC
ELECTE
AUG 4 1989
S A D

APPROVED FOR PUBLIC RELEASE; DISTRIBUTION UNLIMITED

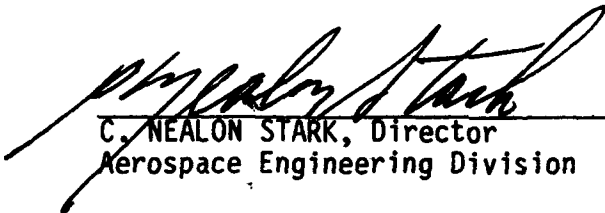
AIR FORCE GEOPHYSICS LABORATORY
AIR FORCE SYSTEMS COMMAND
UNITED STATES AIR FORCE
HANSCOM AIR FORCE BASE, MASSACHUSETTS 01731-5000

"This technical report has been reviewed and is approved for publication"


ROBERT J. RAISTRICK
Contract Manager
Data Systems Branch
Aerospace Engineering Division


ROBERT E. MCINERNEY, Chief
Data Systems Branch
Aerospace Engineering Division

FOR THE COMMANDER


C. NEALON STARK, Director
Aerospace Engineering Division

This report has been reviewed by the ESD Public Affairs Office (PA) and is releasable to the National Technical Information Service (NTIS).

Qualified requestors may obtain additional copies from the Defense Technical Information Center. All others should apply to the National Technical Information Service.

If your address has changed, or if you wish to be removed from the mailing list, or if the addressee is no longer employed by your organization, please notify AFGL/DAA, Hanscom AFB, MA 01731. This will assist us in maintaining a current mailing list.

Do not return copies of this report unless contractual obligations or notices on a specific document requires that it be returned.

Unclassified

SECURITY CLASSIFICATION OF THIS PAGE

REPORT DOCUMENTATION PAGE

1a. REPORT SECURITY CLASSIFICATION Unclassified			1b. RESTRICTIVE MARKINGS	
2a. SECURITY CLASSIFICATION AUTHORITY			3. DISTRIBUTION / AVAILABILITY OF REPORT Approved for public release; distribution unlimited	
2b. DECLASSIFICATION / DOWNGRADING SCHEDULE			5. MONITORING ORGANIZATION REPORT NUMBER(S) AFGL-TR-89-0038	
4. PERFORMING ORGANIZATION REPORT NUMBER(S)			7a. NAME OF MONITORING ORGANIZATION Air Force Geophysics Laboratory	
6a. NAME OF PERFORMING ORGANIZATION RDP, Incorporated		6b. OFFICE SYMBOL (If applicable)	7b. ADDRESS (City, State, and ZIP Code) Hanscom Air Force Base Massachusetts 01731-5000	
6c. ADDRESS (City, State, and ZIP Code) 486 Totten Pond Road Waltham, MA 02154		9. PROCUREMENT INSTRUMENT IDENTIFICATION NUMBER F19628-87-C-0039		
8a. NAME OF FUNDING / SPONSORING ORGANIZATION		8b. OFFICE SYMBOL (If applicable)	10. SOURCE OF FUNDING NUMBERS	
8c. ADDRESS (City, State, and ZIP Code)		PROGRAM ELEMENT NO. 62101F	PROJECT NO. 9993	TASK NO. XX
				WORK UNIT ACCESSION NO. YM
11. TITLE (Include Security Classification) Offaxis Radiance Studies for Infrared Sensors				
12. PERSONAL AUTHOR(S) Mazzella, Andrew J., Jr., Lacaire, Steven A.				
13a. TYPE OF REPORT Scientific No. 1		13b. TIME COVERED FROM 2/3/87 TO 2/2/88	14. DATE OF REPORT (Year, Month, Day) 27 December 1988	15. PAGE COUNT 48
16. SUPPLEMENTARY NOTATION				
17. COSATI CODES			18. SUBJECT TERMS (Continue on reverse if necessary and identify by block number)	
FIELD	GROUP	SUB-GROUP	Infrared sensors; earth-limb measurements; Offaxis response profiles	
04	01			
17	05			
19. ABSTRACT (Continue on reverse if necessary and identify by block number) Offaxis response profiles were developed for the ZIP/ELC and SPIRE infrared sensors, and earth-limb offaxis radiance calculations were performed. Other sources of interfering infrared radiation for earth-limb measurements were also examined.				
20. DISTRIBUTION / AVAILABILITY OF ABSTRACT <input checked="" type="checkbox"/> UNCLASSIFIED/UNLIMITED <input type="checkbox"/> SAME AS RPT <input type="checkbox"/> DTIC USERS			21. ABSTRACT SECURITY CLASSIFICATION Unclassified	
22a. NAME OF RESPONSIBLE INDIVIDUAL Robert J. Raistrick			22b. TELEPHONE (Include Area Code) (617) 377-3726	22c. OFFICE SYMBOL LCY

CONTENTS

INTRODUCTION	1
PROGRAM LOWFILT	1
PROGRAM OAREJ	2
Description of the Computation in OAREJ	2
Extending LOWTRAN4 computed radiance for vehicle altitude = 256 km to other vehicle altitudes	6
MODEL DEVELOPMENT FOR SENSORS	7
CONTAMINANT INVESTIGATIONS	8
 SPIRE OFFAXIS STUDIES	9
 ZIP AND ELC STUDIES	22
ATMOSPHERIC EMISSION	22
BASELINE RADIANCE VARIATION	25
PARAMETRIC OFFAXIS RESPONSE MODELS	30
 CONCLUSION	35
 Appendix A	36
 Appendix B	38
 Appendix C	39
 Appendix D	41
 References	43



INTRODUCTION

The calculation of offaxis radiance for a sensor involves two programs, LOWFILT and OAREJ, and a set of data files specifying the sensor spectral response, sensor offaxis rejection response, and the radiance profile for the earth limb. For this description, the earth limb profile is provided as data generated by the LOWTRAN4 program (reference 1), although more recent or alternative limb profile data could be used, provided the data format is preserved.

For this study, a series of models of offaxis response functions has been developed to characterize the performance of several infrared sensors, including the ZIP telescopes, which were used for both the ZIP (reference 2) and ELC missions, and the SPIRE telescope. A number of observational and theoretical considerations were incorporated into the development of these models, and comparisons of the computed offaxis in-band radiance to actual flight data have been performed. Further investigations are still in progress.

PROGRAM LOWFILT

The program LOWFILT convolves the radiance output of LOWTRAN4 with the spectral response curve of the sensor. The spectral filter response function is provided to LOWFILT as a sequential text file.

The LOWTRAN data provided to LOWFILT has the following characteristics:

- (a) LOWTRAN4 was run in the RADIANCE mode (IEMISS=1);
- (b) the spectral range is 350 inverse-cm to 4200 inverse-cm in steps of 5 inverse-cm;
- (c) there are 25 lines-of-sight designated by 25 tangent heights (TH), or equivalently by 25 zenith angles (BETAP) ranging from 90 degrees to 180 degrees;
- (d) the nominal detector altitude is 256 km;
- (e) the mid-latitude summer model was used, with the boundary layer temperature at the earth's surface determined either by the temperature of the lowest atmospheric layer ("warm-earth" model) or specified independently ("cold-earth" model).

These data are provided to LOWFILT on the file LOSMODL.

The spectral filter function data is provided to LOWFILT on the sequential text file FILTERS. The number of spectral channels to be used must be specified as the first value (NCHANS) in FILTERS, and the number of limb-data sets provided from LOWTRAN4 must be specified as the second value (NFILES) in FILTERS, on the same line as NCHANS. If no value for NFILES is provided, NFILES is assumed to be 25.

LOWFILT generates an output file LOSFILT, which contains the in-band radiance for each spectral channel and for each line-of-sight. LOWFILT also produces a listing.

PROGRAM OAREJ

A computer program, OAREJ, calculates the off-axis in-band radiance from the earth's atmosphere measured by a sensor as a function of

- (a) sensor altitude,
- (b) tangent height or zenith angle for the line-of-sight, and
- (c) wavelength interval.

The program utilizes data from LOWTRAN4 (in the file LOSFILT), as processed through LOWFILT to incorporate the sensor spectral response characteristics, and also requires a data file (OARCURV) containing the sensor off-axis rejection weights.

The product of the sensor off-axis rejection weights and the in-band radiance of the earth's atmosphere is numerically integrated over a solid angle in OAREJ. Because the off-axis rejection function is computed relative to the sensor line-of-sight, the coordinate system used in LOWTRAN to compute the radiance must be related to the sensor coordinates to yield radiance values compatible with the sensor coordinate system before the integration is performed in OAREJ.

A subroutine is included in OAREJ to accommodate different sensor altitudes. This option permits the user to run LOWTRAN at a fixed sensor altitude and then obtain off-axis results for a variety of sensor altitudes. It is assumed that all sensor altitudes are external to the LOWTRAN model atmosphere (above 100 km).

Description of the Computation in OAREJ

In Figure 1, the unprimed axes define the sensor coordinate system and the primed axis define the coordinate system in which the radiance from the earth's atmosphere is calculated. The origin of the two coordinate systems is the sensor position; the z' -axis is the local zenith and the z -axis is the sensor line of sight; B is the angle from the local zenith to the line of sight.

The transformation from the sensor to the radiance coordinates can be written as

$$(1) \quad \begin{aligned} x' &= x \cos B + z \sin B \\ y' &= y \\ z' &= -x \sin B + z \cos B \end{aligned}$$

In terms of spherical coordinates (p, ϕ, θ) where p is the distance, θ the azimuth angle, and ϕ the polar angle, the transformation can be rewritten as

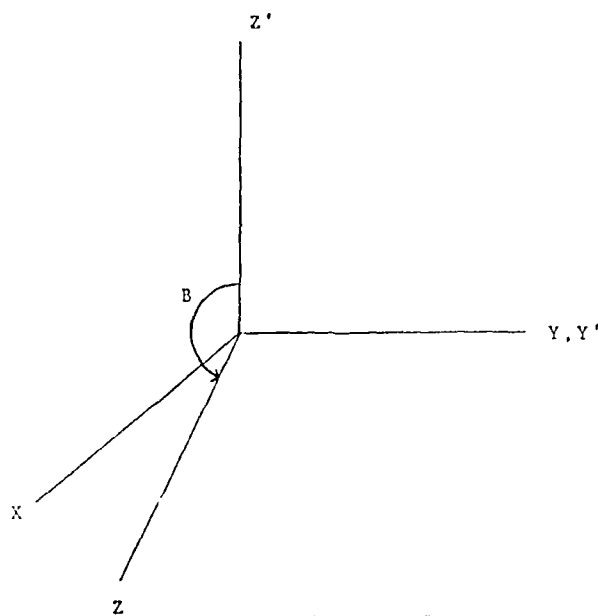


Figure 1

$$\begin{aligned}
 \sin \phi' \cos \theta' &= \sin \phi \cos \theta \cos B + \cos \phi \sin B \\
 (2) \quad \sin \phi' \sin \theta' &= \sin \phi \sin \theta \\
 \cos \phi' &= -\sin \phi \cos \theta \sin B + \cos \phi \cos B
 \end{aligned}$$

In these equations, the polar angle ϕ , specifying a sensor offaxis direction, is measured from the sensor axis (the line-of-sight), while the azimuthal angle θ for the offaxis direction is measured about the sensor axis from the nadir. The polar angle ϕ' , in the coordinates for the atmosphere, is the zenith angle with respect to the local vertical, while θ' is the azimuthal angle about the local vertical.

Only the last equation in (2)

$$(3) \quad \cos \phi' = \cos \phi \cos B - \sin \phi \cos \theta \sin B$$

is required in the off-axis radiation calculations because the atmospheric radiance is assumed to be independent of the azimuthal angle about the local vertical.

In the sensor coordinates, the off-axis radiation measured by the sensor as a function of B , the angle from the zenith to the line of sight, is given by

$$(4) \quad \text{OAR}(B) = \int \int W(\phi, \theta) I(\phi'(\phi, \theta, B)) \sin \phi \, d\phi \, d\theta$$

where $\sin \phi \, d\phi \, d\theta = \text{differential solid angle}$,

$W(\phi, \theta)$ = point source off-axis rejection function of the sensor,
 $I(\phi')$ = in-band radiance of the earth's atmosphere (Watts/sq cm-sr),
 and $I(\phi')$ as a function of ϕ , θ , and B is defined through equation (3).

Equation (4) can be rewritten as

$$(5) \quad \text{OAR}(B) = \int d\phi \sin \phi \int W(\phi, \theta) I(\phi') d\theta,$$

where the sensor offaxis response function $W(\phi, \theta)$ is assumed to be zero for sensor polar angles (ϕ) greater than 90 degrees, and the response function is also assumed to be symmetric in the sensor azimuthal angle θ : $W(\phi, \theta) = W(\phi, -\theta)$.

Numerical integration of equation (5) is performed in the computer program using the trapezoidal method.

As shown in Figure 2, the zenith angle B and the tangent height TH are related by

$$(6) \quad \sin(180^\circ - B) = \sin B = (TH + RE)/(H + RE)$$

where

H = the altitude of the sensor and
 RE = the radius of the earth.

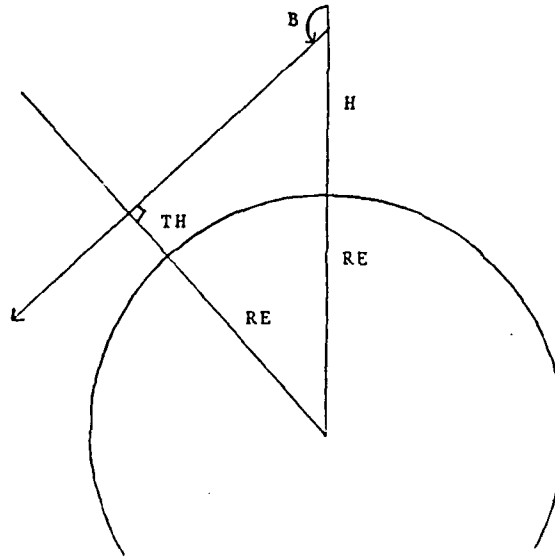


Figure 2

In the computation of $\text{OAR}(B)$ in equation (5), one problem is to determine the values of

$I(\phi, \theta, B)$ from the tabulated values $I(\phi')$, which were computed using LOWTRAN4 and LOWFILT for a specified set $\{\phi'\}$.

The program OAREJ uses the values

$$\begin{aligned} &\phi'(1), \text{RAD}(1) \\ &\phi'(2), \text{RAD}(2) \\ &\cdot \\ &\cdot \\ &\phi'(L), \text{RAD}(L) \end{aligned}$$

and maps each line-of-sight zenith angle $\phi'(k)$ from the interval $[90^\circ, 180^\circ]$ to the interval $[0, 1]$ by means of a negative cosine mapping. An interpolation of the in-band radiance value onto a grid interval of 0.001 in the cosine is included in the mapping process. The relation (3) is used as a map of (ϕ, θ) to $-\cos \phi'$ and hence an in-band radiance value (I) is associated with (ϕ, θ, B) .

Values $W(\phi(i), \theta(j))$ of the off-axis rejection function are supplied to OAREJ as a sequential text file. For each fixed $\phi(i)$, OAREJ uses one of several options to generate interpolated values of $W(\phi(i), \theta)$ for the required azimuthal angles θ . The option chosen is related to the number of $\theta(j)$ values supplied.

Finally, equation (5) is computed as follows:

$$\begin{aligned} G(\phi) &= \int_{-\pi}^{\pi} d\theta W(\phi, \theta) I(\phi, \theta, B) \\ &= 2 \int_0^{\pi} d\theta W(\phi, \theta) I(\phi, \theta, B) \\ &= 2 \sum_{k=0}^K W(\phi, \theta(k)) I(\phi, \theta(k), B) \Delta\theta(k) \end{aligned}$$

where

$$\begin{aligned} \theta(k) &= 0.1 \times k \text{ degrees, for } 0 \leq k \leq K, \\ \Delta\theta(0) &= 0.05 \text{ degree,} \\ \Delta\theta(K) &= 0.05 \text{ degree,} \\ \Delta\theta(k) &= 0.1 \text{ degree, for } 0 < k < K. \end{aligned}$$

The upper limit of the summation ($K \leq 1800$) is determined by the value of θ (if any) which gives a horizontal line-of-sight (zenith angle of 90 degrees) for the specified ϕ . If a horizontal line-of-sight is not attained for any azimuthal angle, then a complete azimuthal integration is performed ($K = 1800$).

Then,

$$\begin{aligned} \text{OAR (B)} &= \int d\phi \sin \phi G(\phi) \\ &= \frac{1}{2} \sum_j [G(j) \sin \phi(j) + G(j+1) \sin \phi(j+1)] \Delta\phi(j). \end{aligned}$$

In addition to computing the total in-band offaxis radiation OAR(B) (Watts/sq cm), the program computes the equivalent offaxis in-band radiance (Watts/sq cm-sr) using the effective field-of-view of the sensor.

Extending LOWTRAN4 computed radiance for vehicle altitude = 256 km to other vehicle altitudes

The standard input to the offaxis rejection program includes radiance values for 25 zenith angles (lines-of-sight) between 90 degrees and 180 degrees and for a vehicle altitude of 256 km. If off-axis radiation results are desired for vehicle altitudes other than 256 km then

- (a) LOWTRAN4 can be rerun for the new vehicle altitude and for appropriate zenith angles, or,
- (b) the LOWTRAN4 256 km results can be interpreted as new vehicle altitude results by observing the relationship between corresponding zenith angles.

Option (b) is valid on the condition that the new altitude remains above the LOWTRAN upper limit of 100 km.

An algorithm for option (b) has been incorporated in the OAREJ program according to the geometry shown in Figure 3. The underlying assumption is that the radiance incident on the sensor A and on sensor B along the indicated line of sight is the same and only depends on TH.

By simple trigonometry,

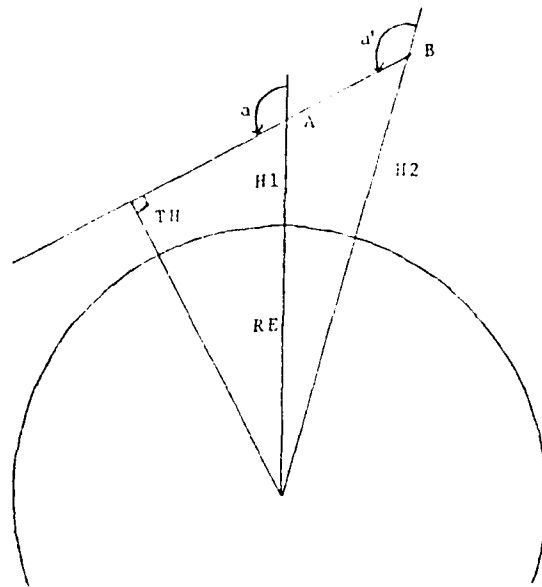
$$\sin a = \sin (180^\circ - a) = (TH + RE)/(H1 + RE)$$

$$\sin a' = \sin (180^\circ - a') = (TH + RE)/(H2 + RE)$$

which implies

$$a' = 180^\circ - \arcsin ((H1 + RE) \sin a / (H2 + RE)).$$

Consequently, radiance values from LOWTRAN for H1=256 km and angle "a" will be the same as the radiance for H2 and angle "a'".



RE = radius of earth

H1 = 256 km

TH = tangent height

Figure 3

MODEL DEVELOPMENT FOR SENSORS

The sensors incorporated in this study are characterized by two complementary performance specifications: the offaxis response function, and the spectral response function. Because the data from the primary sensor (SPIRE) investigated in this study is spectral in nature, the spectral response functions used could be very simply characterized as flat responses over distinct wavelength intervals. The computed results could then be directly compared to definite integrals over portions of the measured spectrum. The offaxis response functions are represented in more detail, but still with some simplification, in that azimuthal symmetry about the sensor axis is assumed.

The four spectral bands used for all of the sensors in this study were:

Band 1: 10.2 μ -12.0 μ

Band 2: 9.2 μ - 10.5 μ
Band 3: 8.8 μ - 9.2 μ
Band 4: 14.0 μ - 16.0 μ

The spectral responses were assigned to be unity within each band, and zero outside of each band.

The ZIP offaxis response profile (reference 2) was initially available for this study, and provided the basis for evaluating the "far-axis" response (offaxis angles beyond 10°) for the SPIRE offaxis response profile. The "near-axis" response for the SPIRE sensor was provided (reference 3) from design specifications and measurements by SSG, Inc. The detector field-of-view was taken to be 1.2×10^{-5} sr, for converting the total flux (Watts/cm²) to an equivalent in-band radiance (Watts/cm²-sr).

CONTAMINANT INVESTIGATIONS

Potential sources of excess radiance for a rocket-borne infrared sensor were also examined, as alternatives to offaxis radiance due directly to the sensor design. The evidence for such sources is indirect, being associated with a spectral, spatial, or temporal dependence which is different from that determined for offaxis radiance. Possible contaminants are:

- 1) vapors or gases escaping from the payload during the measurements, producing a local infrared emission;
- 2) particulate material associated with the payload, producing a local infrared emission as well as scattering of earth or solar radiation;
- 3) vapors or particles that escape from the payload and condense onto the mirror surfaces of the sensor, degrading the offaxis response, but in a time-dependent manner.

Both the ZIP and ELC flights were examined for such effects.

SPIRE OFFAXIS STUDIES

The initial SPIRE offaxis response is shown in Figure 4. The principal characteristics of this profile are the ϕ^{-3} dependence for the response below 3.5 degrees, the small "plateau" region between 3.5 and 6.5 degrees, represented as an exponential dependence for the offaxis response, the two transition segments to 30 degrees, also represented by exponentials, and the final "roll-off" from 30 degrees to zero response at 90 degrees. The response from on-axis to 6.5 degrees is the measured response particular to the SPIRE sensor, with the shape of the extended response being based on model data originally provided by SSG for the ZIP sensor. The ϕ^{-3} dependence for the near-axis response is characteristic of a diffraction response, while the transition region is indicative of the sensor design and the quality of the mirrors.

The primary results calculated for this offaxis response function are the offaxis in-band radiance versus tangent height for the line-of-sight for each spectral band, at specified altitudes for the sensors. These were compared to the radiance "floor" observed in the flight data for the initial evaluation of the offaxis response model. The preliminary SPIRE offaxis response model produced an offaxis radiance floor that was too low by about a factor of 30 to correspond to the actual measurements, but a "worst case" SPIRE offaxis response model, corresponding to a degraded mirror with an offaxis response varying as $\phi^{-3/2}$ for offaxis angles beyond 3 degrees, produced an offaxis radiance floor that was too large by a factor of 30.

The large uncertainty in the far-axis offaxis response performance prompted an investigation into the location of the sources of the incident offaxis radiance. This is a function not only of the location of the strong emitters, but also of the attenuating effects of the offaxis response function.

A preliminary indication of the radiation source was explored by eliminating essentially all infrared emission from the solid body of the earth, leaving only atmospheric emission from a relatively thin shell. For this case, the LOWTRAN model was run using a temperature of 10° K as the earth temperature, while the lowest atmospheric boundary layer had the standard temperature for the mid-latitude summer model. The relative emission intensities for the cold earth to warm earth models were approximately 30% for Band 1, 34% for Band 2, 27% for Band 3, and 100% for Band 4, for lines-of-sight intersecting the solid earth. Lines-of-sight not intersecting the solid earth were unchanged. The absence of change for Band 4 is a consequence of the atmosphere being optically thick for this CO₂ band.

A further investigation into the radiation source locations was performed by examining the offaxis flux incident on the detector for each of the zones used for the polar angle integration. A sample plot is given in Figure 5, for three of the bands used with the initial SPIRE offaxis response profile. Discontinuities in the zonal profile result from the changes in the polar zone widths, but the predominance of the contribution between polar angles of

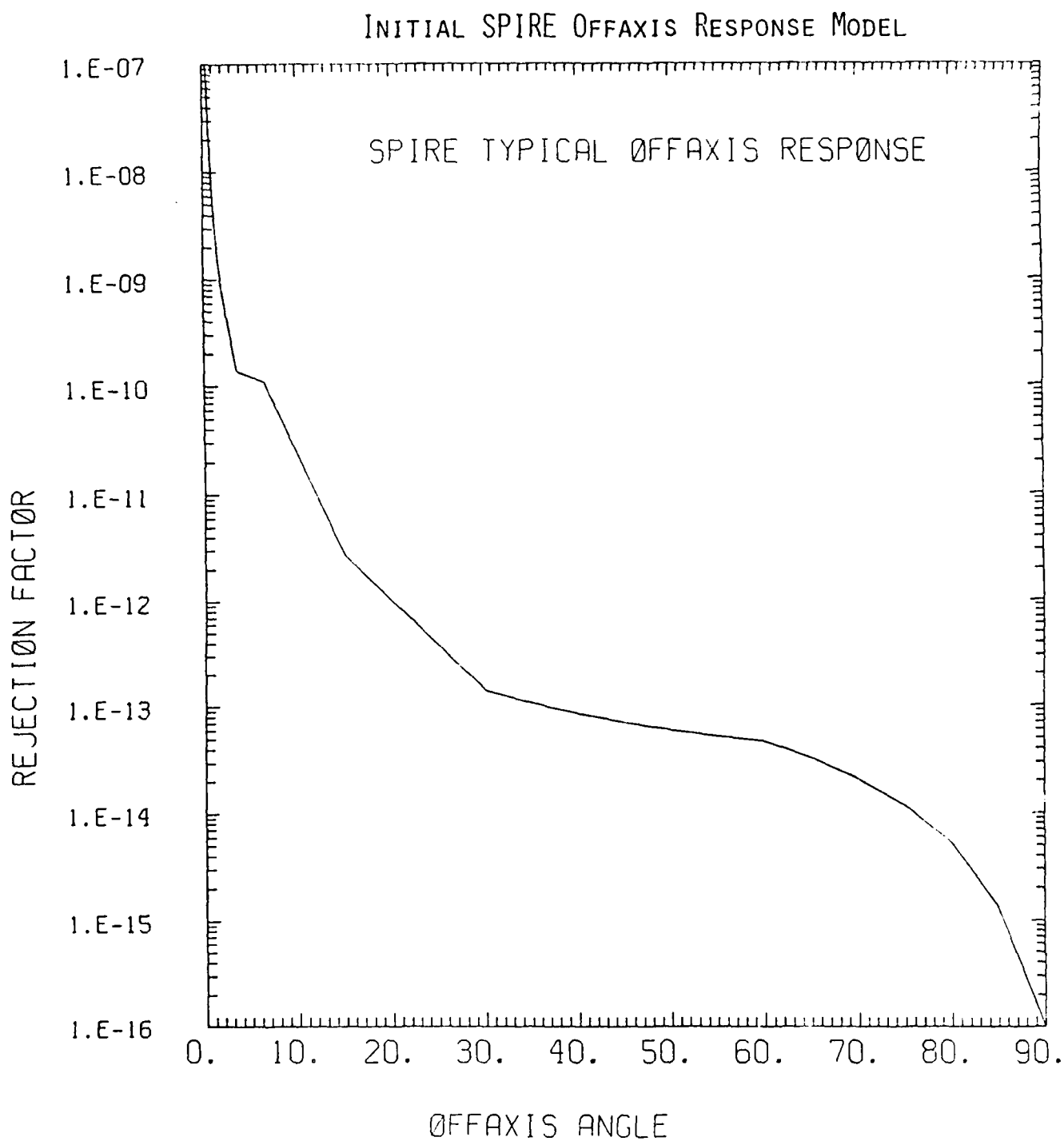


Figure 4

5 and 10 degrees is evident.

Based on these preliminary results, a new offaxis response profile, designated "SPIRE Model A", was developed. The near-axis performance of the initial SPIRE offaxis profile was retained, but the response beyond 10 degrees was modified to be intermediate between the initial SPIRE offaxis profile and the worst case SPIRE offaxis profile. This profile is displayed in Figure 6.

The results of the offaxis in-band radiance calculations for the SPIRE Model A are displayed in Figures 7-10. The calculated radiance "floor" is below the data baseline by approximately a factor of three for Bands 1 and 2, and a factor of fifteen for Band 3, but is above the data baseline by approximately a factor of 4 for Band 4. The data baseline is noise-dominated for Band 3, so that the actual radiance baseline may be lower, and, consequently, the discrepancy from the calculated offaxis in-band radiance would be less. The discrepancy between Bands 1 and 2 and Band 4 is also difficult to reconcile with possible offaxis response profiles, based on the zonal distribution of the offaxis radiance.

An alternative SPIRE offaxis response complementary to SPIRE Model A was also developed, and was designated as SPIRE Model B. This offaxis response profile retained the response of the initial SPIRE offaxis model beyond 6.5 degrees, but joined immediately to the near-axis diffraction response, without the plateau transition. This produced a degraded near-axis response relative to the initial SPIRE model (see Figure 11). The calculated offaxis radiance results are significantly different from both the SPIRE Model A results and the flight data in both magnitude and tangent height dependence.

Further investigation was then conducted into the offaxis response for the transition region, corresponding to polar angles between 6 and 30 degrees. Some constraints on the offaxis response for these polar angles were available from SPIRE vertical scans which were within 15 degrees of the sun, although there was considerable uncertainty in the local azimuth for these scans. The preliminary expectation was that excess radiance observed during these scans was offaxis radiance from the sun, which would be a localized source at a specific offaxis polar angle, so that an actual in-flight measurement of the offaxis response profile over some range of polar angles could be performed.

The uncertainty in the azimuth of the scans complicated this derivation, in that the exact polar angle for the sun was not known, and a further complication was the presence of an additional on-axis radiance source, the zodiacal light. This is a wavelength-dependent background whose intensity varies with the angle of the line-of-sight from the sun and also from the ecliptic plane. The pointing uncertainty for the SPIRE sensor thus also translates into an uncertainty in the zodiacal light estimate. However, the absence of a zodiacal light excess in the measured data also allowed limits to be derived for the azimuth of the SPIRE vertical scans.

SPIRE 'Typical' Case Offaxis Response

Vehicle Altitude: 150 km

Tangent Height of LOS: 100 km

Zenith Angle of LOS: 97.0996

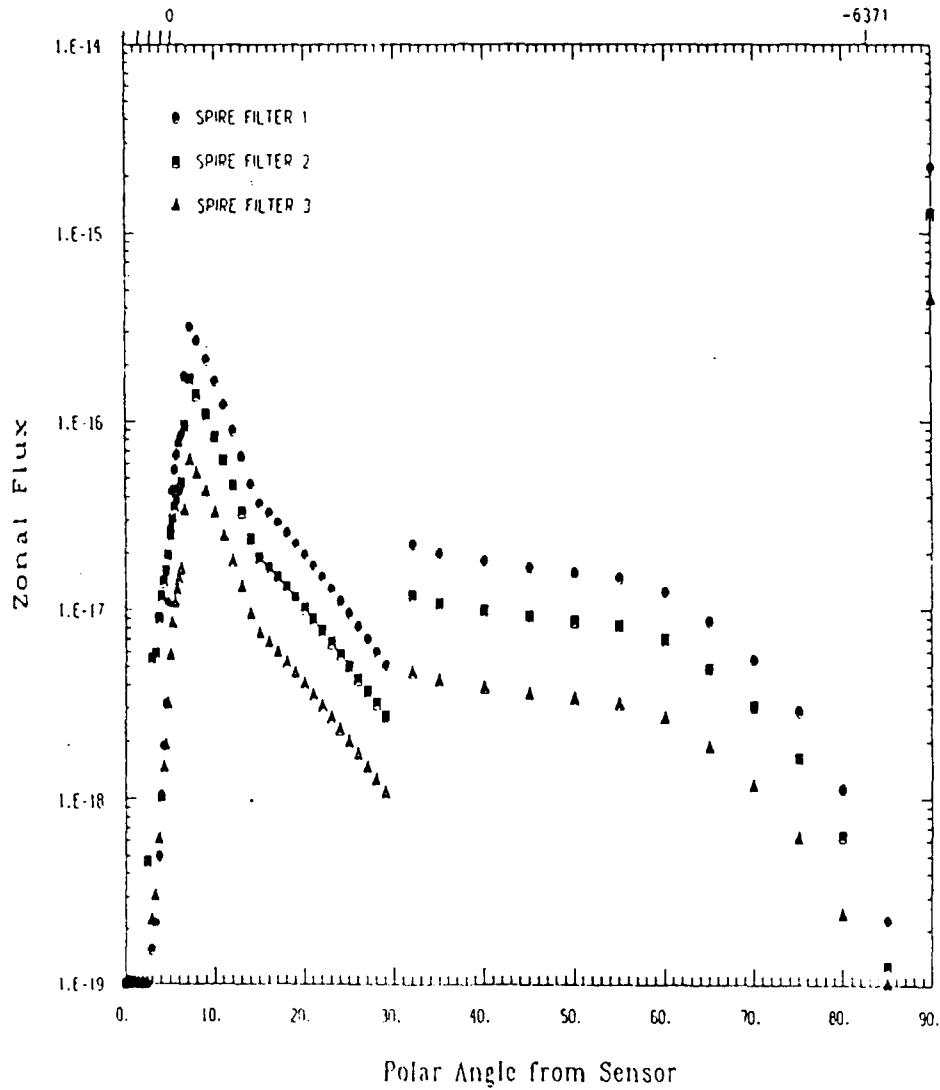


Figure 5

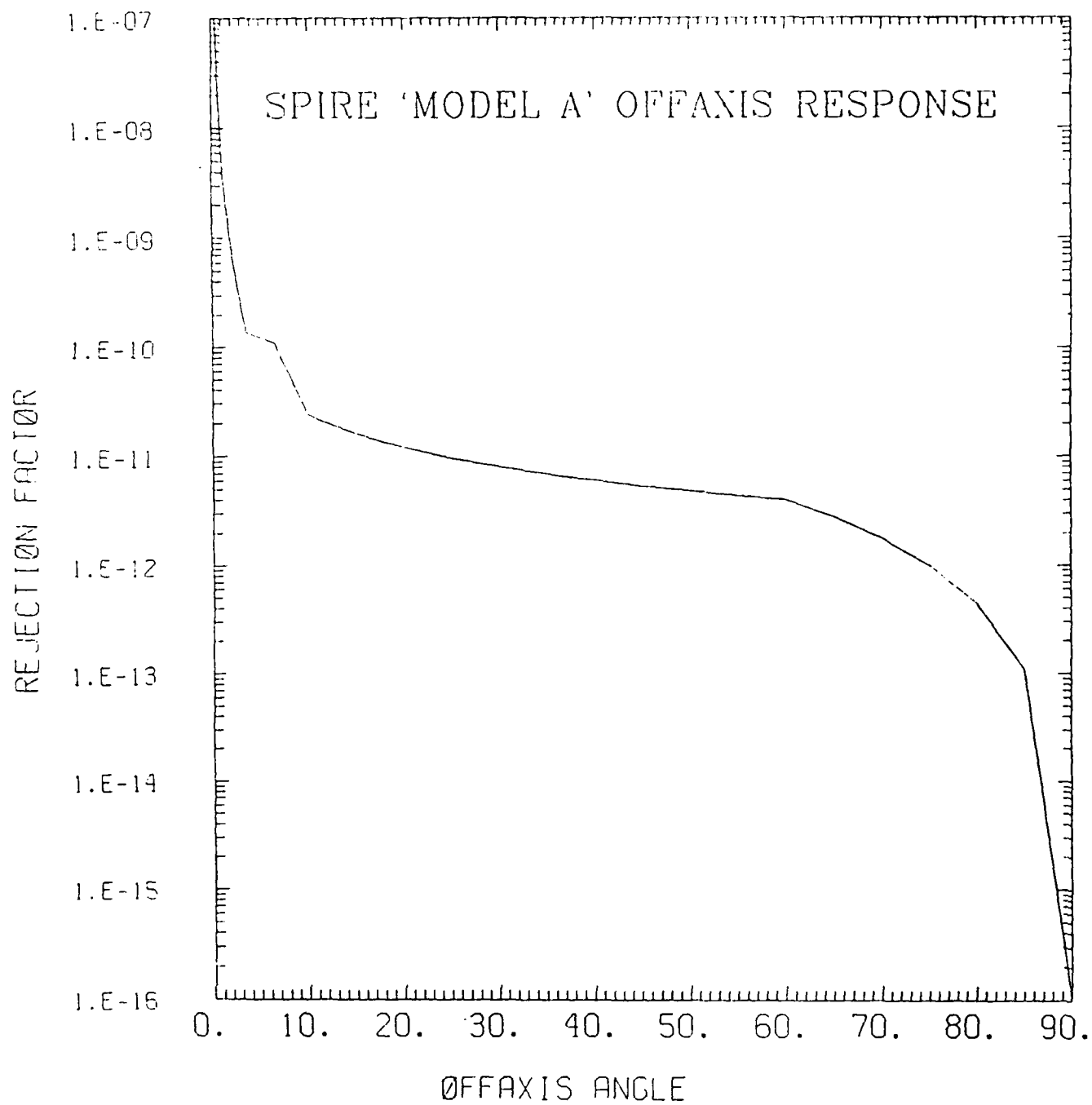


Figure 6

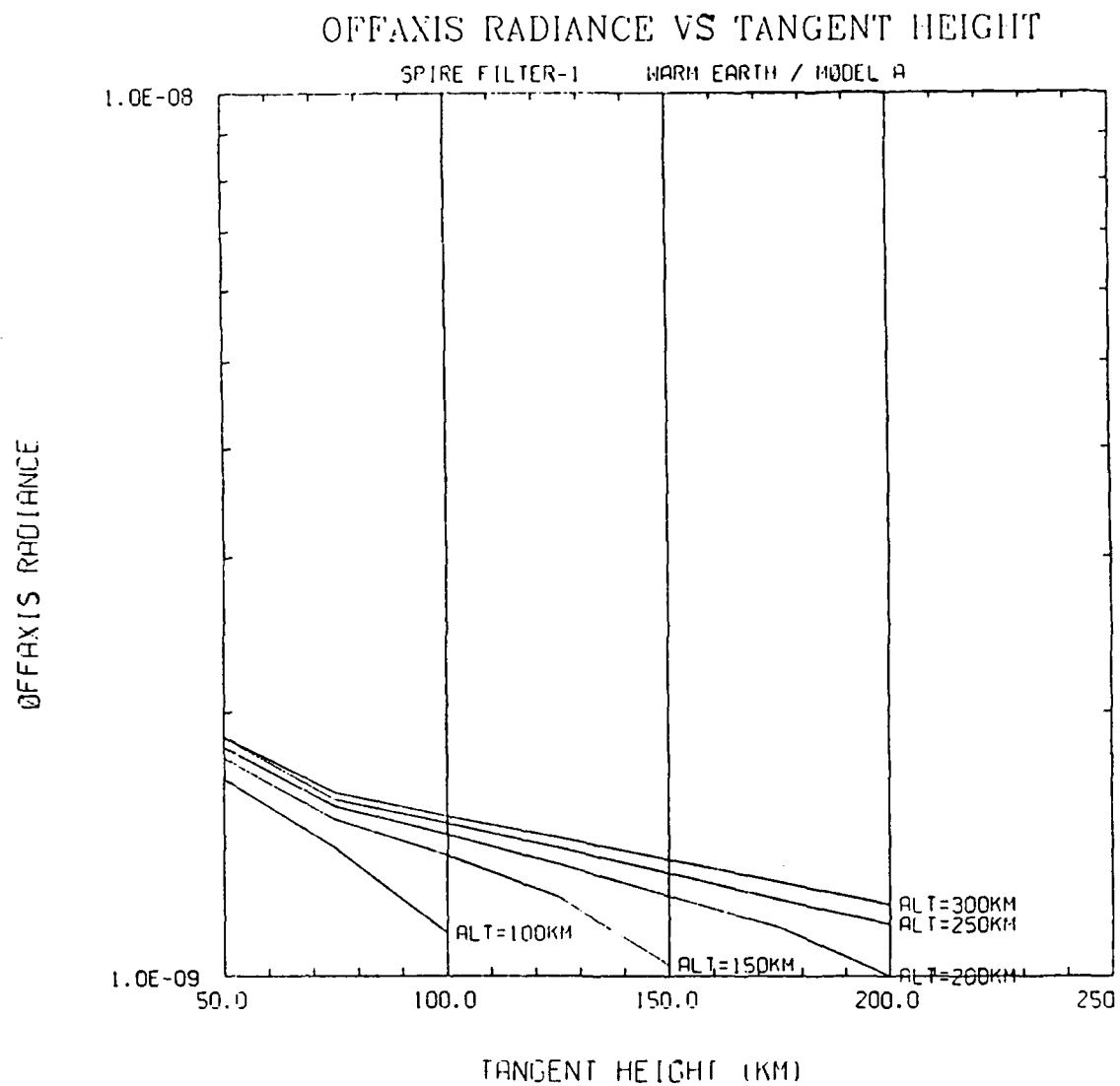


Figure 7

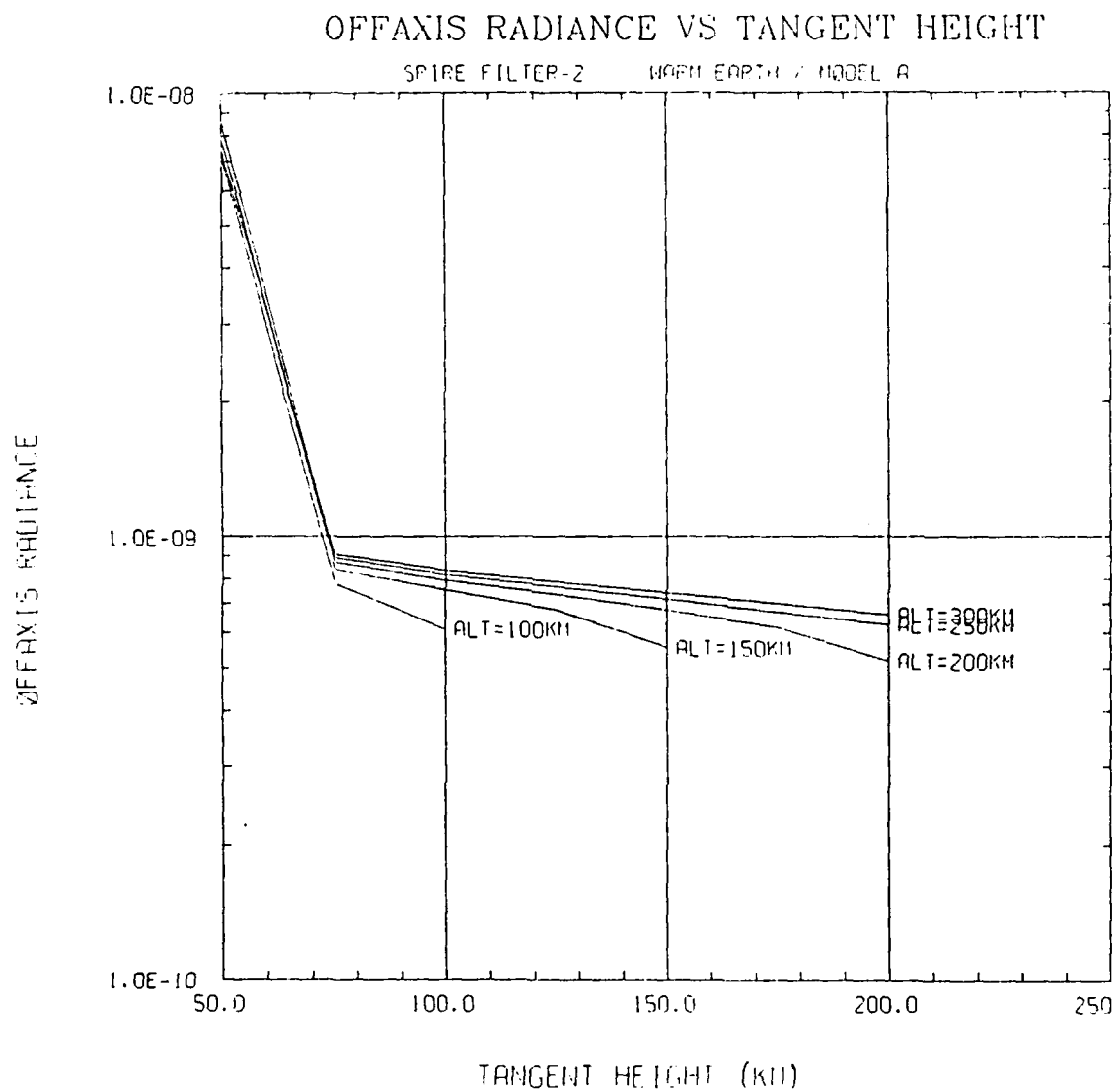


Figure 8

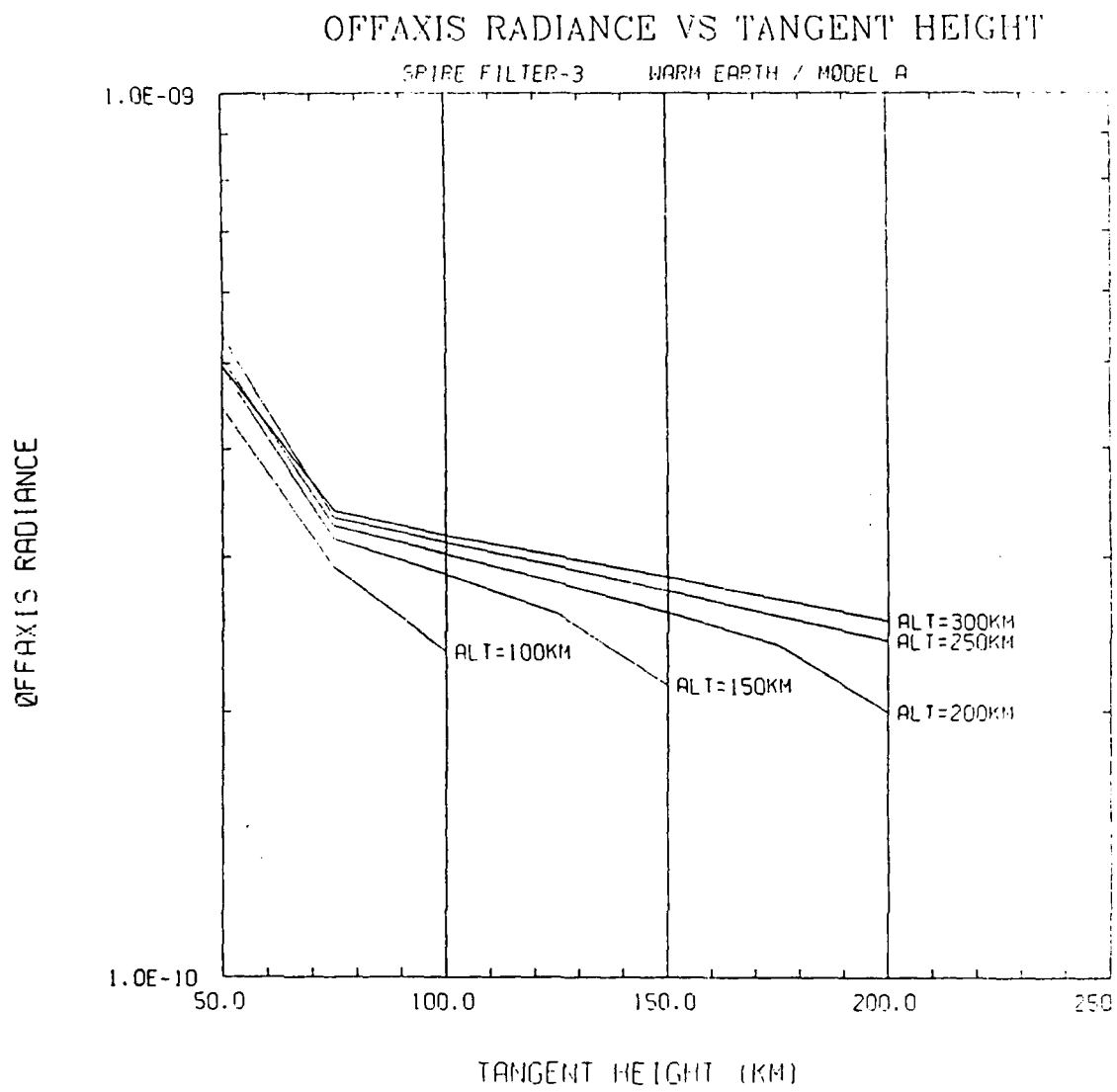


Figure 9

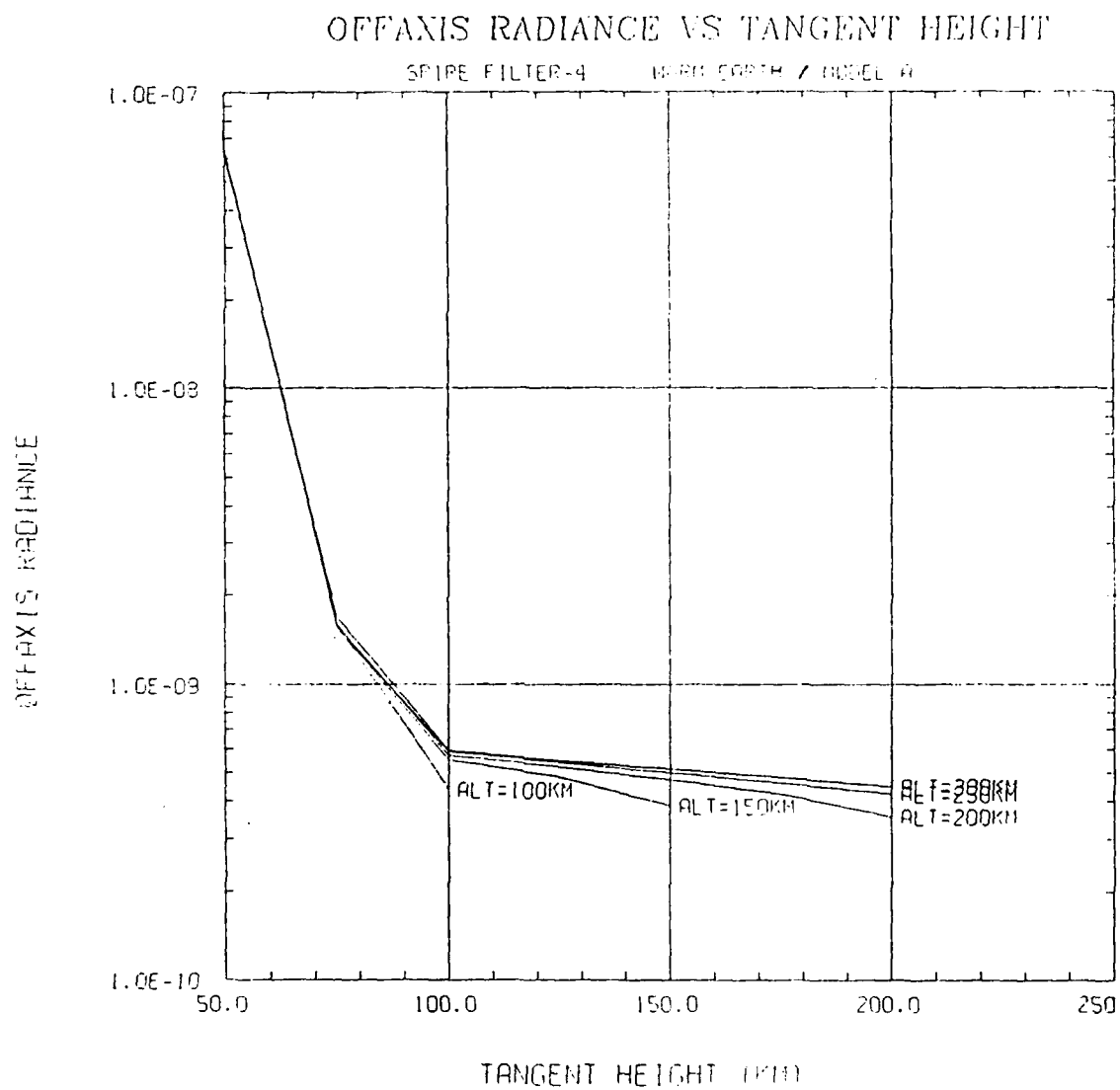


Figure 10

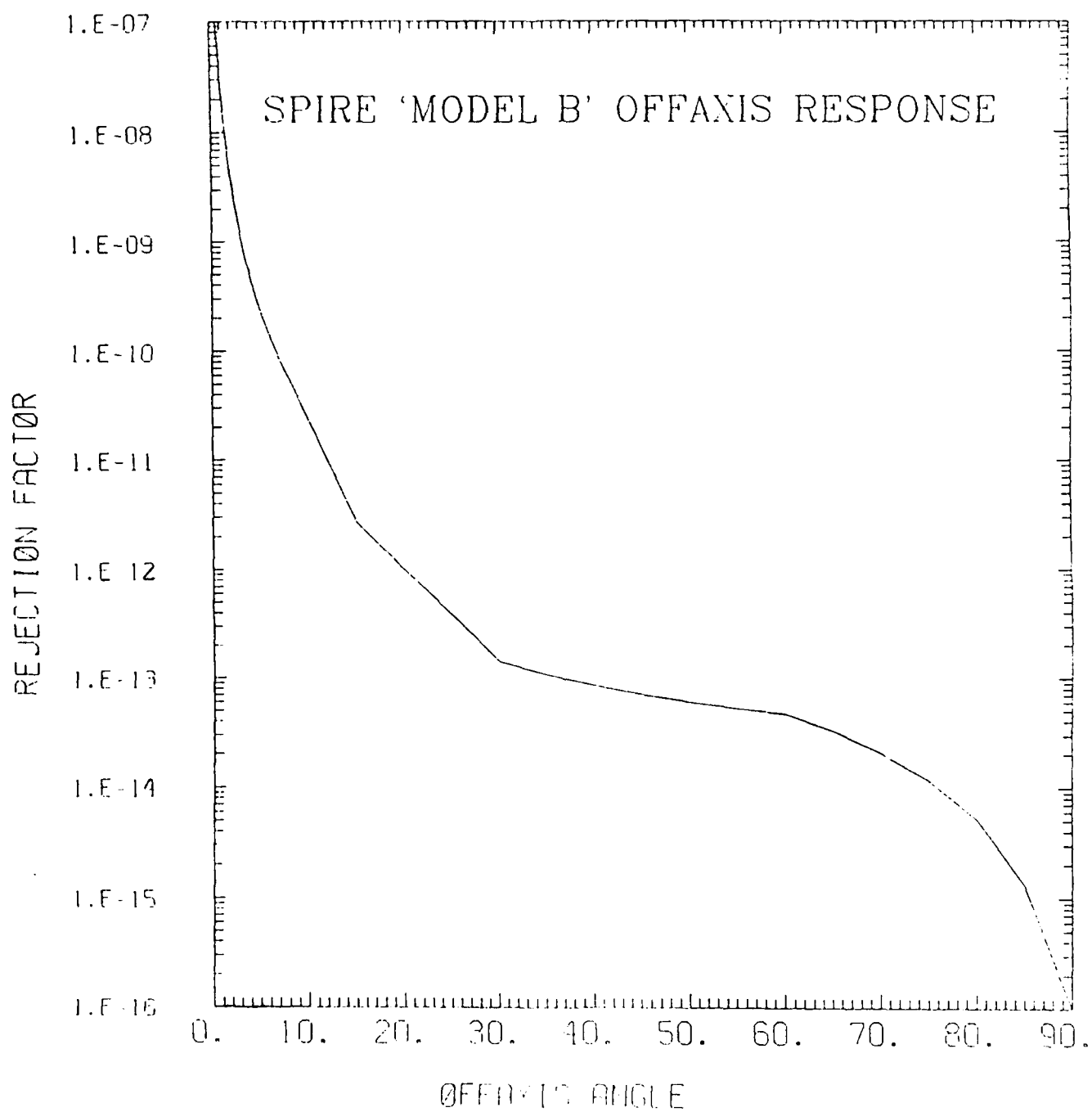


Figure 11

The ZIP zodiacal model (reference 2) was used to calculate the zodiacal light for Bands 1 and 2 for angles between 2 and 18 degrees from the sun. These values were compared to the excess in-band radiance values observed for vertical scans 9 and 12 for the SPIRE flight, taken with respect to "standard" vertical scans which were known to be far from the sun. In particular, vertical scans 3 and 8 were used as reference scans. The results of this comparison are displayed stepwise in Table 1.

Solar Offaxis Determination

(All in-band radiance values are Watts/cm²-sr)

Excess scan radiance

	Band 1	Band 2
Scan 9	5.0×10^{-9}	5.0×10^{-9}
Scan 12 (120 km)	1.5×10^{-8}	1.4×10^{-8}
Scan 12 (132 km)	8.2×10^{-8}	9.0×10^{-8}

Zodiacal light

	Band 1	Band 2
3°	2.3×10^{-8}	2.4×10^{-8}
6°	9.8×10^{-9}	9.8×10^{-9}
9°	5.8×10^{-9}	5.5×10^{-9}
12°	3.8×10^{-9}	3.6×10^{-9}
15°	2.7×10^{-9}	2.5×10^{-9}

Solar offaxis in-band radiance estimate (excess minus zodiacal light)

Scan 9

	Band 1	Band 2
12°	1.2×10^{-9}	1.4×10^{-9}
15°	2.3×10^{-9}	2.5×10^{-9}

Scan 12 (120 km)

	Band 1	Band 2
6°	5.0×10^{-9}	4.0×10^{-9}
9°	9.0×10^{-9}	8.0×10^{-9}
12°	1.1×10^{-8}	1.0×10^{-8}
15°	1.2×10^{-8}	1.2×10^{-8}

Scan 12 (132 km)

	Band 1	Band 2
3°	6.7×10^{-8}	5.8×10^{-8}
6°	8.0×10^{-8}	7.2×10^{-8}
9°	8.4×10^{-8}	7.6×10^{-8}
12°	8.6×10^{-8}	7.8×10^{-8}

Solar offaxis rejection factor estimate

Scan 9

	Band 1	Band 2
12°	4.1×10^{-10}	4.2×10^{-10}
15°	7.9×10^{-10}	7.6×10^{-10}

Scan 12 (120 km)

	Band 1	Band 2
6°	1.7×10^{-9}	1.2×10^{-9}
9°	3.1×10^{-9}	2.4×10^{-9}
12°	3.8×10^{-9}	3.0×10^{-9}
15°	4.1×10^{-9}	3.6×10^{-9}

Scan 12 (132 km)

	Band 1	Band 2
3°	2.3×10^{-8}	1.8×10^{-8}
6°	2.8×10^{-8}	2.2×10^{-8}
9°	2.9×10^{-8}	2.3×10^{-8}
12°	3.0×10^{-8}	2.4×10^{-8}

Table 1

The results of this offaxis response evaluation are displayed in Figure 12, together with the corresponding modifications in the SPIRE offaxis response profile. This revised profile has been designated as SPIRE Model C, but no offaxis in-band radiance calculations for the earth limb have yet been performed for it.

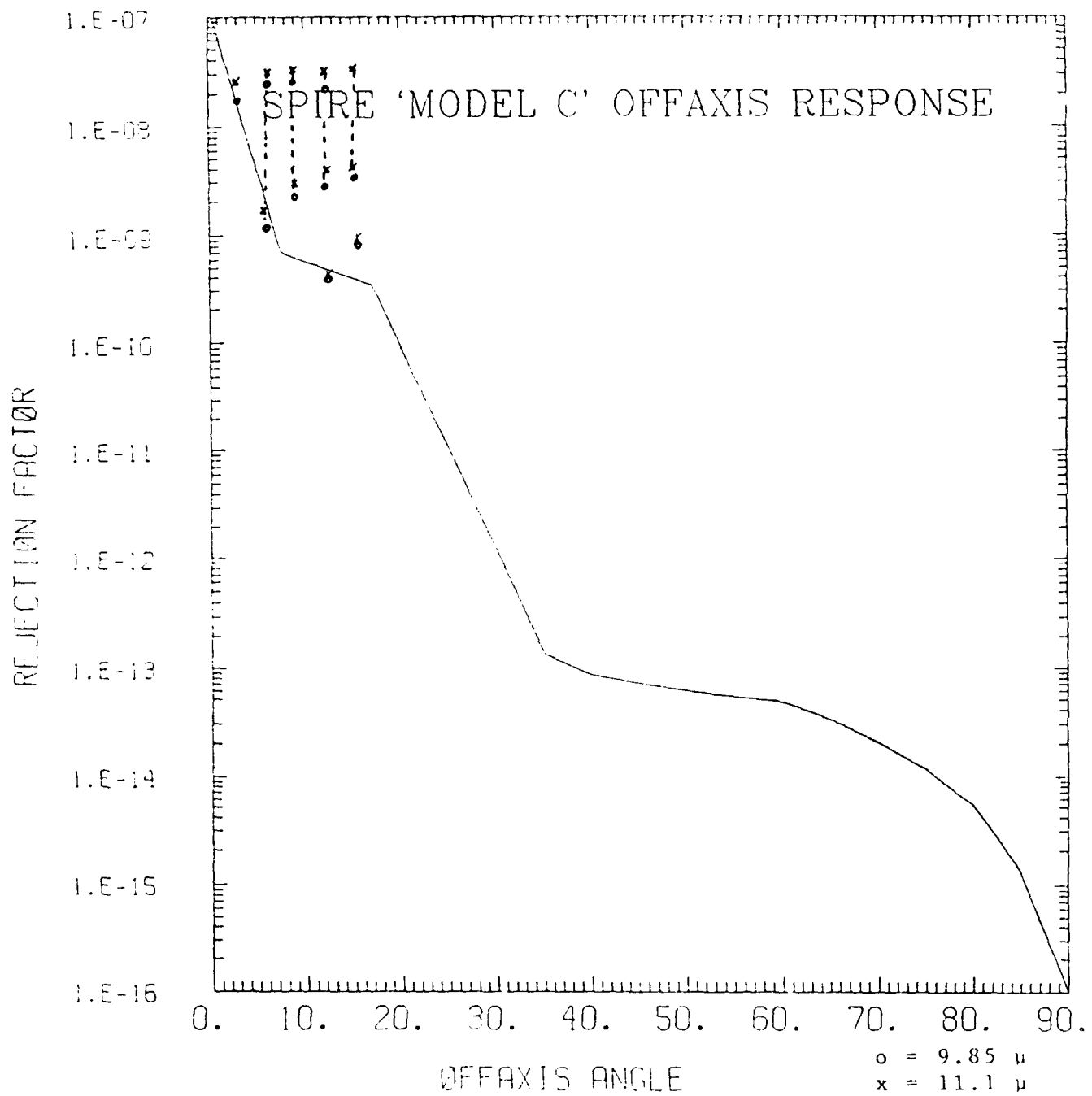


Figure 12

ZIP AND ELC STUDIES

The ZIP (Zodiacal Infrared Project) and ELC (Earth Limb Clutter) experiments consisted of three rocket flights for two nearly identical infrared sensors, with further differences in the infrared filter bands and detector configurations in the focal planes of the ZIP and ELC instruments. The ZIP measurements were performed for strictly upward-looking lines-of-sight, while the ELC measurements were performed for horizontal and downward-looking lines-of-sight. The trajectories for the ZIP-1 and ELC flights remained completely within the earth's shadow, but the ZIP-2 payload passed out of the earth's shadow during its ascent, scanned to within 17° of the sun, and then re-entered the earth's shadow during its descent.

An offaxis response profile (Figure 13) was developed for the ZIP sensor during the course of the ZIP data analysis, and this profile was used for both earth limb and solar offaxis radiance calculations. The maximum earth limb offaxis radiance calculated using this model was less than 10^{-12} Watts/cm²-sr- μ , while the maximum solar offaxis radiance is 4.4×10^{-11} Watts/cm²-sr- μ for ZIP detectors 1 and 2 (2.99μ), 2.2×10^{-11} Watts/cm²-sr- μ for detectors 3 and 4 (5.95μ) and 5 and 6 (6.11μ), and no greater than 2×10^{-12} Watts/cm²-sr- μ for any of the other detectors.

Excess radiance features were observed on both ZIP flights, however, and were attributed to the following sources:

- a) A spatially localized feature in ZIP-1 was determined to be the plume from the tumbling, unspent rocket booster;
- b) A spatially localized feature in ZIP-2 was regarded as being a fragment from the separation system;
- c) A diffuse time-dependent excess radiance was decomposed into altitude-dependent and temporally-decreasing elements, which were regarded as atmospheric emission and payload outgassing, respectively. The parameters characterizing both of these elements were different for the two ZIP flights.

The atmospheric emission model was re-examined in this study in conjunction with the earth limb offaxis radiance calculations, and the ZIP-2 data was reviewed to determine upper limits for the possible solar offaxis radiance.

ATMOSPHERIC EMISSION

The atmospheric emission models for the ZIP flights were derived in a similar manner for both flights, although details of the derivation process differed between the two flights because of differences in the flight scanning profiles. In both flights, a scan performed during the atmosphere re-entry segment covered the same region of the celestial sphere as an earlier scan, performed when the payload was at a higher altitude. The celestial background, consisting of both zodiacal and galactic emission, would thus be the same for both scans, so that the difference in radiance levels would be attributed to a local effect,

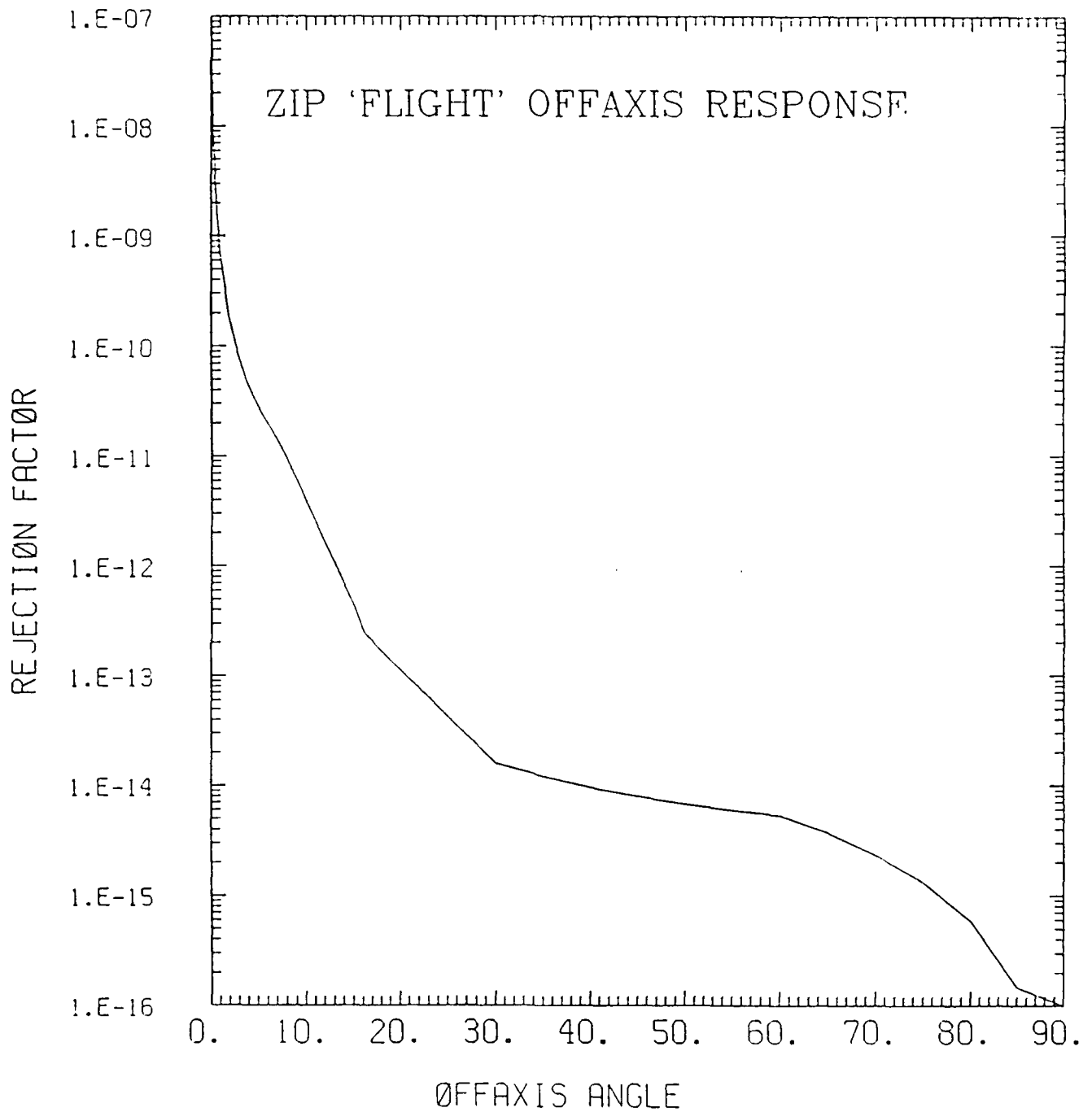


Figure 13

which was regarded as being the intervening atmosphere. This difference in radiance level was fit by an exponential in altitude, with corrections for the zenith angle of the line-of-sight with respect to the local vertical. The results for both flights, given as the scale height h_0 and the reference radiance A at an altitude of 170 km, are presented in Table 2.

ZIP Atmosphere Model Parameters

$$R = (A/\cos z)\exp(-(h - h_r)/h_0)$$

for R in pico-Watts per square centimeter per steradian per micron.

z = zenith angle for line-of-sight;

A = atmosphere radiance at reference altitude;

h_r = reference altitude (170 km);

h_0 = scale height (km);

h = payload altitude.

Channel	ZIP-1		ZIP-2	
	A	h_0	A	h_0
1	-	-	-	-
2	-	-	-	-
3	98.7278	28.2413	249.7880	15.2124
4	87.1600	28.0800	225.6547	15.2124
5	73.7223	25.6809	106.6931	13.0213
6	136.1800	25.0000	-	-
7	17.1712	23.2391	42.8333	9.9819
8	21.2977	23.8938	51.3990	10.3253
9	19.4181	27.8842	27.0214	17.9292
10	21.5499	27.0995	28.9713	22.0513
11	10.0041	24.0849	-	-
12	14.6367	25.6915	25.5500	13.3435
13	6.1219	39.5946	14.8657	14.0120
14	7.2225	33.4495	29.7313	14.0120
15	15.4068	44.4325	34.2405	19.2915
16	14.2341	37.2367	36.3062	15.3417
17	3.4052	46.0517	10.7282	10.5796
18	4.8820	40.0882	10.7282	10.5796
19	3.8197	37.8932	10.7282	10.5796
20	3.2402	31.6101	10.7282	10.5796
21	0.9949	42.8524	3.0500	11.8765
22	2.2049	53.7329	3.0500	11.8765
23	2.0535	59.8587	2.6564	11.7371
24	2.8615	44.1038	3.4409	11.9348

25	1.9571	128.2007	17.1471	10.1847
26	2.2022	87.4550	5.4404	10.1847
27	2.9365	41.6452	5.3211	7.0546
28	3.2754	45.1801	10.5239	18.2498
29	3.7929	46.1233	5.9218	9.2215
30	3.3422	39.3053	5.9651	9.2215

Table 2

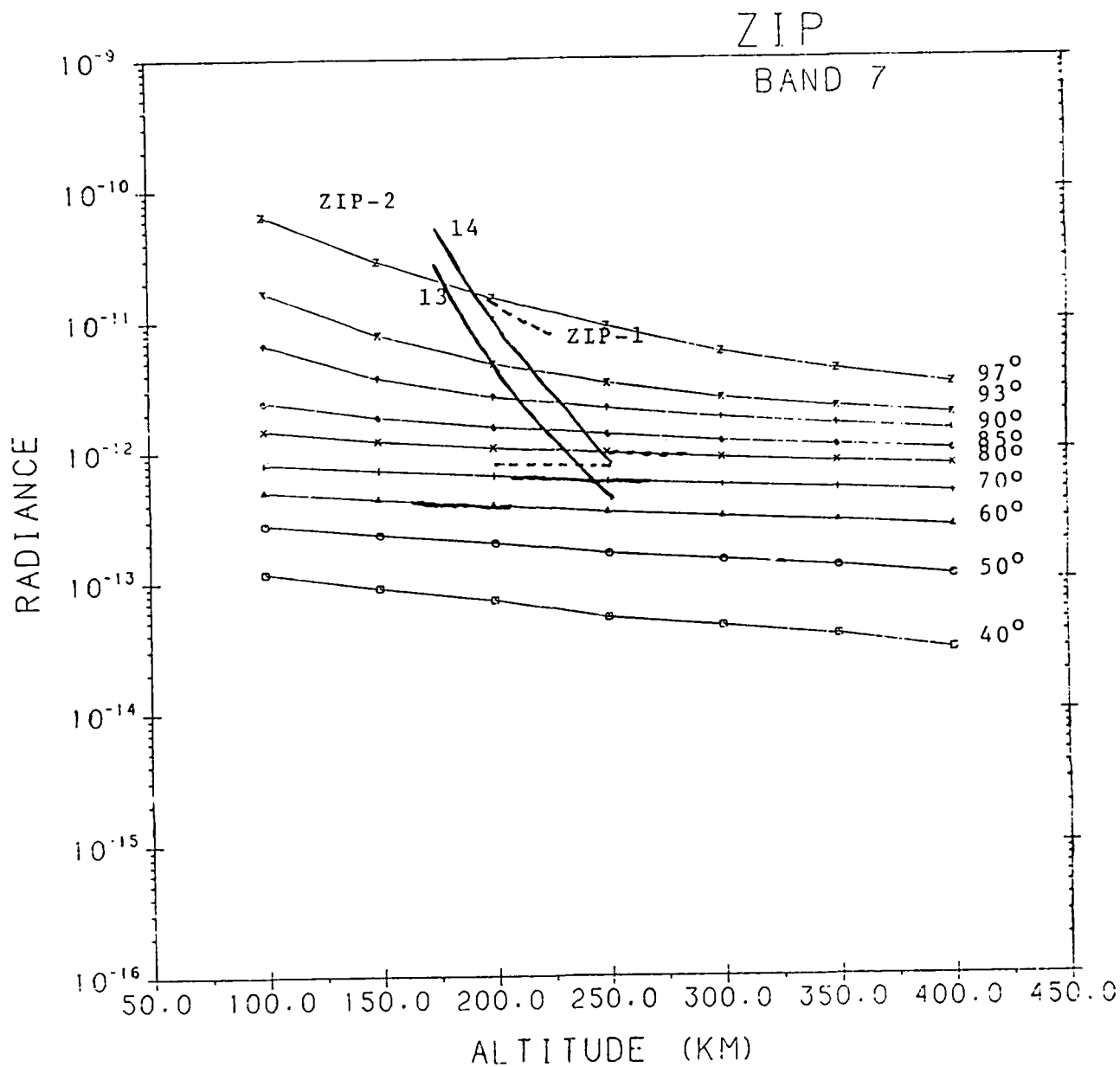
The results for the atmospheric radiance model were examined in conjunction with earlier offaxis radiance calculations performed for a series of sensor altitudes (see Figure 14), to determine whether the radiance attributed to on-axis atmosphere might not actually be offaxis radiance corresponding to a degraded offaxis response profile. This possibility remains an open question, because the calculated offaxis radiance values are less than those of the atmosphere model, but the shapes of the two radiance profiles are distinctly different. Thus, more than a scaling factor change over an extended region of the offaxis profile is required to achieve a correspondence between the two results, and a distinct change in the shape of the offaxis response profile is indicated.

The ELC experiment was intended to measure atmospheric radiance, and therefore the ELC lines-of-sight are either horizontal or downward. It is primarily from the near-horizontal lines-of-sight that the offaxis radiance effects would be observed, and these occur mostly at the beginning or end of the vertical scans, for which the pointing determination is not as accurate as for the tilted scans, which consist of only downward-looking lines-of-sight.

A number of plots of atmosphere profiles, representing in-band radiance versus tangent height, were studied. These plots represented different wavelength bands as well as different segments of the flight. For a number of cases, the in-band radiance displays a flat or very shallowly decreasing dependence on increasing tangent height, for tangent heights of the order of 180 km to 220 km, with the in-band radiance values being substantially above those corresponding to the noise level of the detectors. This characteristic is considered to be offaxis in-band radiance, but corresponds to a sensor performance significantly worse than that predicted from the ZIP offaxis response profile, which should be reasonably valid for the ELC sensor.

BASELINE RADIANCE VARIATION

The monotonically time-dependent component of the ZIP radiance measurements was derived after the atmospheric model, so that atmospheric effects during the ascending portion of the flights could be removed first. The process was not a straightforward one for



ZIP Atmosphere Models (Steep Slopes)
Compared to Calculated Offaxis Radiance for Zenith Angles
40° to 90°
[Actual ZIP Zenith Angles Shown Darker]

Figure 14

the ZIP-2 flight, however, as the reference celestial background scan was still affected by the time-dependent baseline, so some iteration was required. This time-dependent component was modelled as a single exponentially decreasing radiance baseline for ZIP-1, and as a double exponential for ZIP-2. The parameters for these models are given in Table 3.

ZIP Baseline Model Parameters

$$R = A \exp(-B(t - t_0)) + C \exp(-D(t - t_0))$$

for R in pico-Watts per square centimeter per steradian per micron.

A, C = baseline radiance coefficients;

B, D = inverse time constants;

t_0 = reference time (170 sec);

ZIP FLIGHT 1

Channel	A	B	C	D
1	-	-	-	-
2	-	-	-	-
3	20.0000	0.0120	10.3000	0.0400
4	20.0000	0.0120	9.2000	0.0400
5	33.7000	0.0140	3.6000	0.0500
6	45.3000	0.0120	5.6000	0.0500
7	43.2300	0.0132	0.0000	0.0000
8	43.4600	0.0144	0.0000	0.0000
9	21.7300	0.0122	0.0000	0.0000
10	20.0300	0.0109	0.0000	0.0000
11	15.9000	0.0109	0.0000	0.0000
12	16.6100	0.0131	0.0000	0.0000
13	12.5900	0.0132	0.0000	0.0000
14	12.5900	0.0132	0.0000	0.0000
15	13.2300	0.0170	0.0000	0.0000
16	14.2800	0.0151	0.0000	0.0000
17	9.7300	0.0112	0.0000	0.0000
18	6.6100	0.0119	0.0000	0.0000
19	6.2900	0.0130	0.0000	0.0000
20	5.6600	0.0130	0.0000	0.0000
21	10.7700	0.0100	0.0000	0.0000
22	6.9300	0.0123	0.0000	0.0000
23	3.7800	0.0268	0.0000	0.0000
24	3.7800	0.0268	0.0000	0.0000
25	0.9100	0.0523	0.0000	0.0000

26	0.9100	0.0523	0.0000	0.0000
27	12.9500	0.0154	0.0000	0.0000
28	15.6400	0.0137	0.0000	0.0000
29	15.1800	0.0163	0.0000	0.0000
30	15.1800	0.0163	0.0000	0.0000

ZIP FLIGHT 2

Channel	A	B	C	D
1	-	-	-	-
2	-	-	-	-
3	68.4300	0.0120	12.3400	0.0500
4	69.2600	0.0120	10.0600	0.0500
5	67.4000	0.0120	5.1500	0.0660
6	-	-	-	-
7	105.6800	0.0112	0.0000	0.0000
8	97.2300	0.0146	0.0000	0.0000
9	33.4700	0.0107	0.0000	0.0000
10	34.6700	0.0108	0.0000	0.0000
11	-	-	-	-
12	26.3200	0.0118	0.0000	0.0000
13	32.3000	0.0138	0.0000	0.0000
14	30.6700	0.0138	0.0000	0.0000
15	24.5100	0.0084	0.0000	0.0000
16	22.3900	0.0136	0.0000	0.0000
17	9.9500	0.0107	0.1500	0.0900
18	6.9900	0.0168	0.1500	0.0900
19	4.6900	0.0186	0.1500	0.0900
20	3.2700	0.0238	0.1500	0.0900
21	7.3400	0.0146	0.3000	0.0900
22	5.9000	0.0150	0.2500	0.0900
23	0.0000	0.0000	0.8200	0.0717
24	0.0000	0.0000	0.8200	0.0720
25	0.0000	0.0000	0.5500	0.0900
26	7.3000	0.0120	0.4900	0.0800
27	10.9400	0.0180	0.2000	0.0900
28	12.6100	0.0180	0.2500	0.0900
29	19.7300	0.0180	0.3500	0.0900
30	17.4400	0.0183	0.2500	0.0900

Table 3

The ELC flight data was examined for a similar phenomenon, although the investigation was complicated by several factors.

- 1) A horizontal line-of-sight prevailed during the initial ascending portion of the flight, so that a significant atmospheric background was directly observed, making any possible baseline variation less conspicuous.
- 2) A large but spatially discrete object was observed during the early portion of the flight, obscuring possible baseline effects.
- 3) The attitude determination for the re-entry portion of the flight was somewhat uncertain, so that a direct comparison of the radiance profiles for the ascending and descending portions of the flight allow a significant margin of error.
- 4) The sensor orientation differed between the ascending and re-entry portions of the flight, so that the offaxis radiance effects may not be identical.

Nevertheless, there is a reasonable correspondence between the ascending and descending portions of the flight (see Figure 15), and a baseline radiance effect of the same order as that observed during the ZIP flights does not appear to be present.

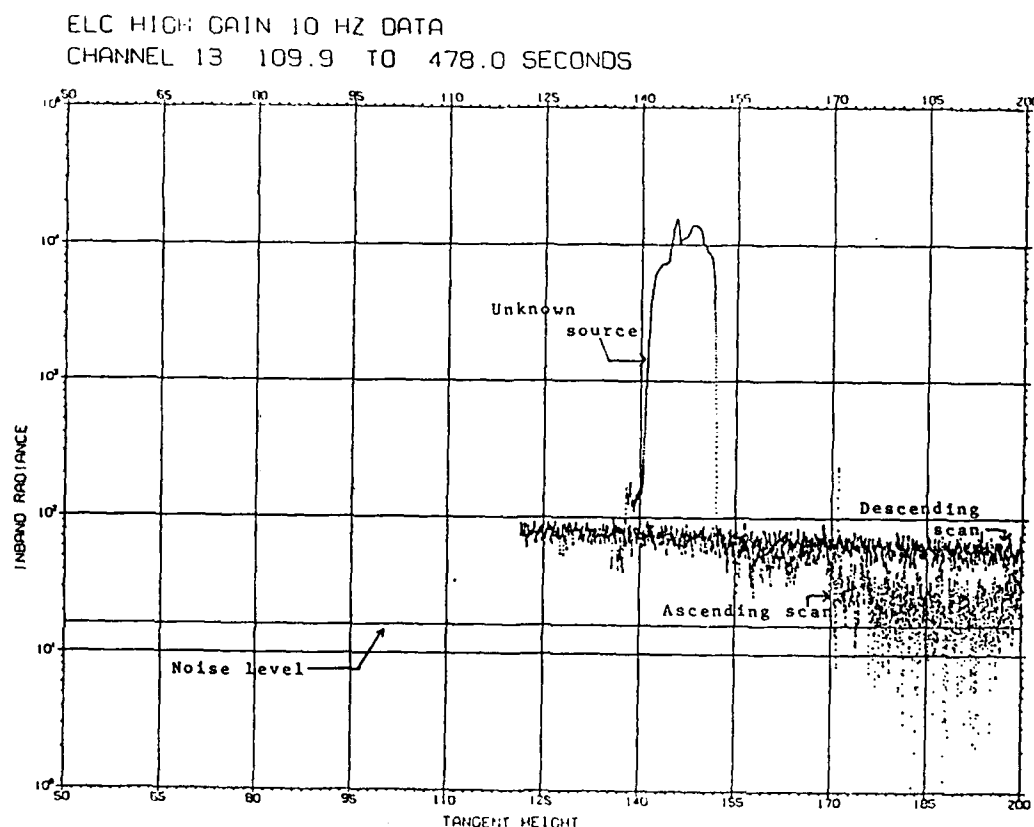


Figure 15

PARAMETRIC OFFAXIS RESPONSE MODELS

The original ZIP offaxis response profile and all of the SPIRE offaxis response profiles were represented by piecewise functional forms over designated ranges of offaxis polar angle. This produces a variety of parameters required to characterize the offaxis response profile and complicates the process of offaxis radiance calculations. Consequently, simpler functional forms were sought which still accurately represent the offaxis response profile and whose parameters are related to basic physical properties of the sensor.

The first parametric functional form implemented for the offaxis response profile was the following:

$$r = [C \cos \phi / (A + \phi^n)] / (1 + (F \phi)^m) + D \cos \phi$$

where

r = offaxis response factor,

C , A , F , and D are fixed coefficients, and

n and m are fixed exponents, associated with the scattering distribution function of the mirrors.

The factor $[C \cos \phi / (A + \phi^n)]$ represents the near-axis response, the term $(D \cos \phi)$ represents the far-axis response, and the inverse factor $(1 + (F \phi)^m)$ characterizes the transition region.

Parameters were derived to characterize the ZIP and SPIRE offaxis response profiles, but it proved difficult to relate these parameters to two quantities that are commonly used to characterize the quality of a mirror for a sensor. These quantities are the Bidirectional Reflectance Distribution Function (BRDF) measured at a polar angle of one degree and the exponent associated with the BRDF.

An alternative formulation developed by J.M. Dowling, which incorporates the BRDF parameters directly and also incorporates additional parameters related to the baffle characteristics of the sensor and secondary scattering characteristics, has been implemented for the ZIP offaxis response profile. Some revisions to the Dowling formulation were incorporated to better represent the baffling for the primary mirror, and to allow for different diameters for the aperture and primary mirror.

The parameters used in the Dowling formula are given in Table 4, together with the values adopted to characterize the published ZIP offaxis response.

Symbol	ZIP Flight value	Description
Ω	6.3×10^{-4}	Detector field-of-view (sr)
A	14.40	Aperture diameter (cm)
M	11.20	Mirror diameter (cm)
L	36.80	Baffle length (cm)
F	3.4×10^4	Diffraction suppression factor
w	1.0×10^{-3}	Effective operating wavelength
B_1	1.0×10^{-4}	BRDF at 1 degree
n	2.0	BRDF power roll-off
K	1.5×10^{-5}	Second-order scattering factor
m	0.0	Exponent for second-order scattering

Table 4

The formulation implemented for the alternative offaxis response parametrization was:

$$r = (180/\pi)^3 (w \Omega / \pi^3) \Phi^3 / (A F) + B_1 \Omega f(\Phi) \Phi^n + B_1 \Omega K \Phi^m \cos \Phi$$

where $f(\Phi)$ is an obscuration factor for the primary mirror baffle and has the form:

$$\begin{aligned} f(\Phi) &= 1, & \text{for } \Phi < \Phi_1; \\ f(\Phi) &= (\beta A^2/M^2 + \alpha - 2 L \tan \Phi \sin \alpha/M)/\pi, & \text{for } \Phi_1 \leq \Phi < \Phi_2; \\ f(\Phi) &= 0, & \text{for } \Phi_2 \leq \Phi. \end{aligned}$$

In these formulas, Φ_1 and Φ_2 represent critical limits on the partial obscuration of the primary mirror, with

$$\begin{aligned} \tan \Phi_1 &= (A - M)/(2 L), \\ \tan \Phi_2 &= (A + M)/(2 L), \end{aligned}$$

and α and β are auxiliary angle parameters defining the illuminated fraction of the primary mirror, with

$$\begin{aligned} \cos \alpha &= [(L \tan \Phi)^2 + (M^2 - A^2)/4]/(M L \tan \Phi) \\ \cos \beta &= [(L \tan \Phi)^2 + (A^2 - M^2)/4]/(A L \tan \Phi). \end{aligned}$$

The aperture and mirror diameters for the ZIP flight model are effective values only, because both of these are shaped as semi-circles. The diffraction suppression factor, second-order scattering factor, and second-order exponent were all determined to match

the calculated response to the flight model. The only significant difference between the ZIP flight model and its representation by Dowling's formula is in the transition region to second-order scattering, where the ZIP flight model response is larger than that calculated by the formula. (See Figure 16.)

A revised ZIP offaxis response profile, designated ZIP Model A, was developed from the ZIP flight rejection profile, using this formulation. For the ZIP Model A, only B_1 and n were changed, with $B_1 = 1.0 \times 10^{-3}$ and $n = 1.5$. (See Figure 17.) This model will be used for further offaxis radiance calculations.

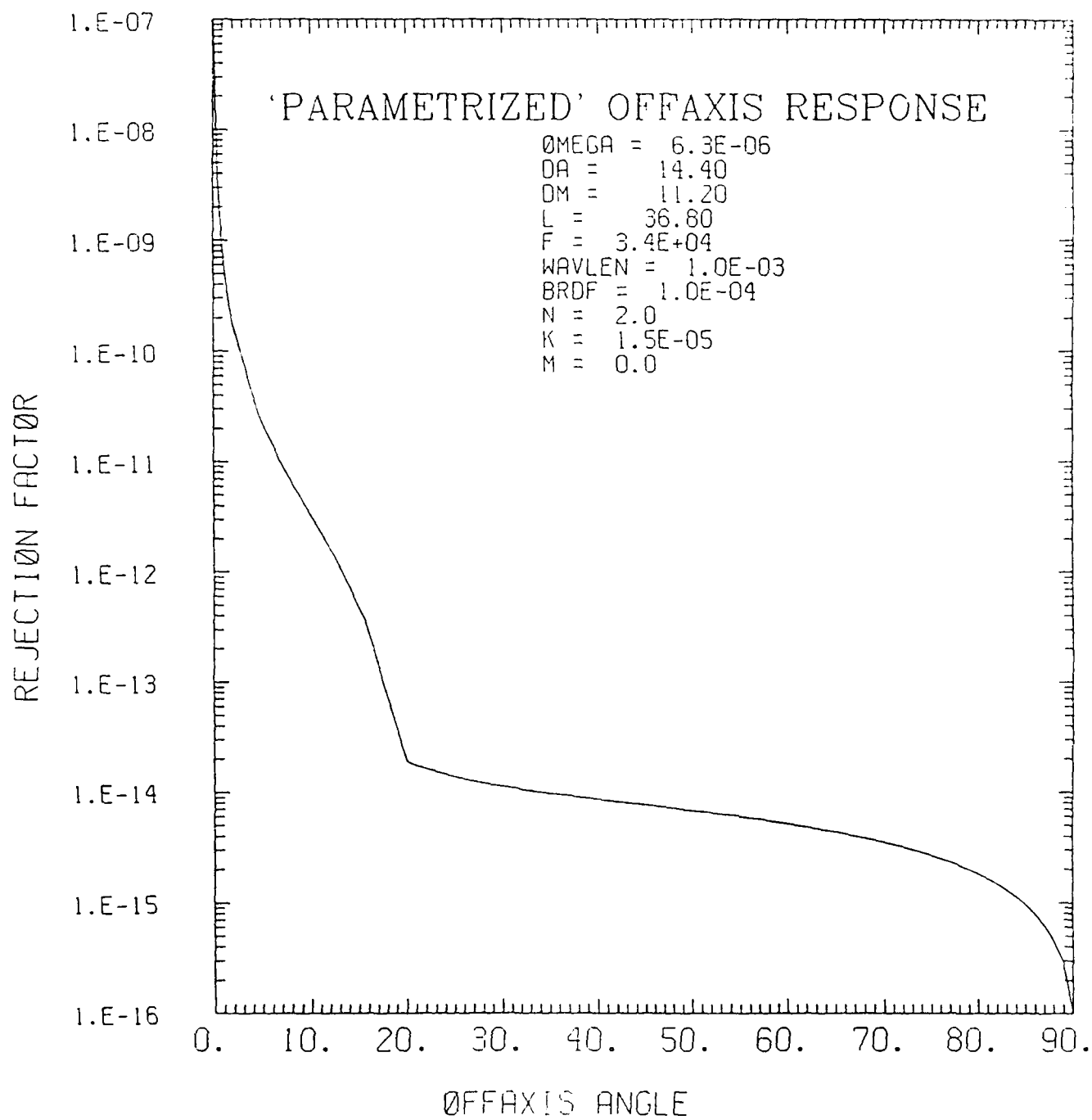


Figure 16

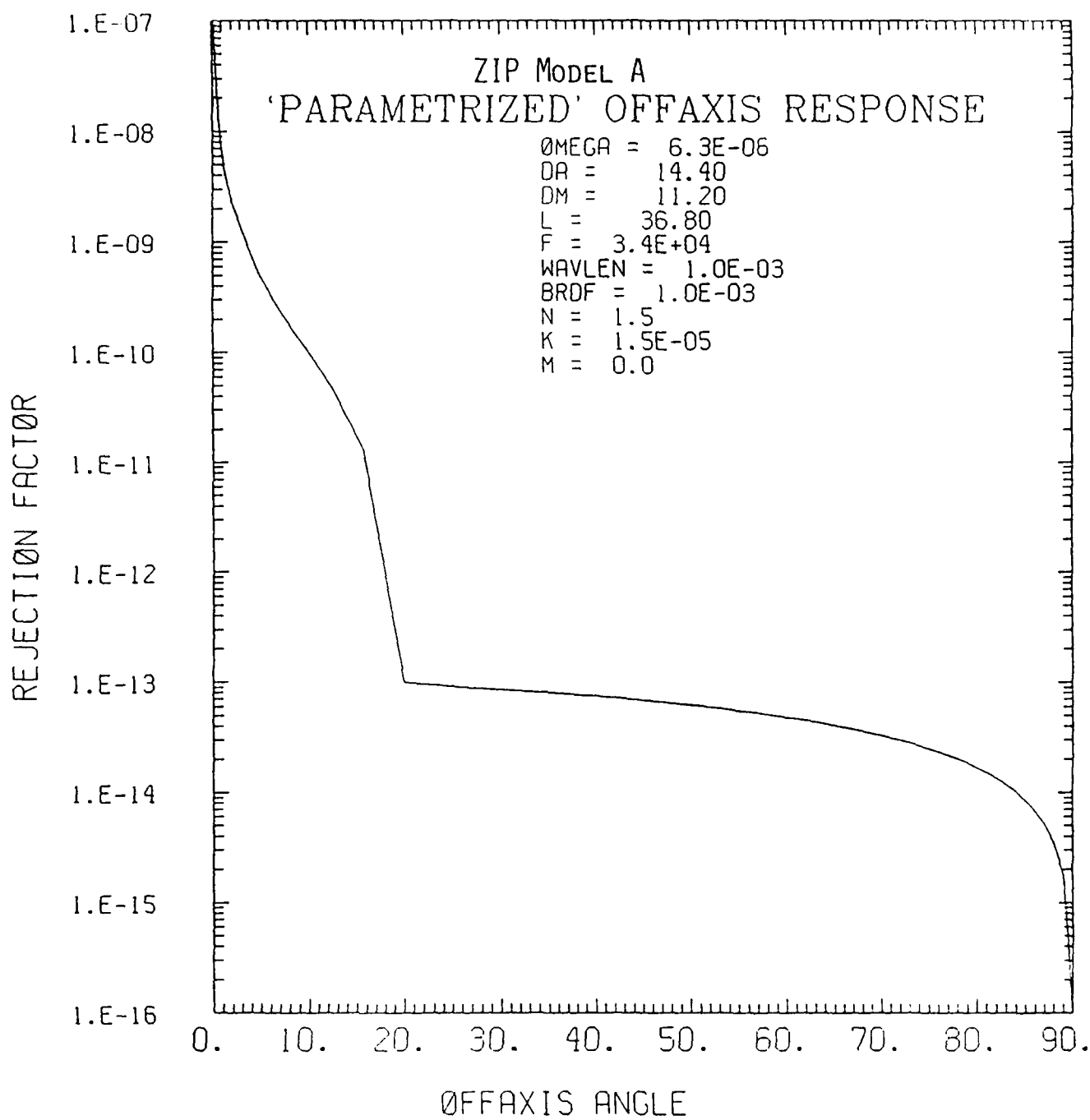


Figure 17

CONCLUSION

The LOWTRAN model and OAREJ program have been utilized to evaluate offaxis radiance for several sensor models, with a general correspondence to radiance profiles actually observed in the sensor data, although detailed agreement is yet to be achieved. The initial estimates of the offaxis response profile for the SPIRE sensor appear to be somewhat optimistic, and a more realistic estimate has been derived, with further refinement yet to be tested. The ZIP/ELC offaxis response profile has been investigated for consistency with data acquired during flight, and a parametric model has been developed for these sensors to investigate the domain of allowable sensor performance within the observational constraints, which are imposed both by observed atmospheric radiance limits and by solar offaxis radiance limits. Atmospheric offaxis effects can be observed in the ELC data, but are less evident for the upward-looking ZIP data.

The possible existence of a localized contaminant has been investigated, but without definite confirmation, except for the effect attributed to payload outgassing during the ZIP flights but which appears to be absent during the ELC flight.

Appendix A

Parameters Used for LOWTRAN 4 Radiance Calculation

MODEL = 2	mid-latitude summer model
IHAZE = 1	aerosol attenuation
ITYPE = 3	vertical or slant path to space
LEN = 0	slant path selection
JP = 0	print transmittance/radiance table
IM = 0	no initial radiosonde data
M1 = 0	no temperature profile modification
M2 = 0	no water vapor profile modification
M3 = 0	no ozone profile modification
ML = 0	no levels for radiosonde model
IEMISS = 1	radiance mode
RO = 0.0	uses earth radius from model (6371.23 km)
TBOUND = 0.0	uses earth temperature from model
H1 = 256.0	sensor altitude
H2 = 0.0	source altitude
ANGLE = 103.234	zenith angles for lines-of-sight (run separately)
103.607	
103.969	
104.323	
104.668	
104.838	
105.006	
105.172	
105.336	
105.499	
105.660	
105.819	
105.977	
106.288	
106.594	
107.189	
107.765	
108.323	
108.865	
112.535	
117.634	
125.857	
138.732	
159.035	

180.000

RANGE = 0.0

not required

BETA = 0.0

not required

VIS = 0.0

sea level visual range

V1 = 350.0

lower frequency range, in inverse-cm

V2 = 4200.0

upper frequency range, in inverse-cm

DV = 5.0

frequency increment for tabulation, in inverse-cm

Appendix B

LOWFILT Input Files

LOSMODL

This file is a concatenation of 25 files generated by LOWTRAN, with one file for each line-of-sight. The first record in each line-of-sight segment is a header record describing the model parameters and the line-of-sight, and contains the following values:

MODEL, IHAZE, ITYPE, H1, ANGLE, HMIN, V1, V2, DV, IEMISS.

All of the above values except HMIN are those provided initially to LOWTRAN4 (see Appendix A), while HMIN is the tangent height for the line-of-sight.

The header record is followed by a sequence of data records describing the spectrum of the atmospheric radiance along the line-of-sight. The values in each record are:

- frequency of the radiation, in inverse-cm;
- radiance at the specified frequency, per inverse-cm;
- radiance at the specified frequency, per micron;
- cumulative radiance, integrated over wave-number;
- total transmittance at the specified frequency;
- water vapor transmittance at the specified frequency.

FILTERS

This file contains a set of specifications for the sensor spectral response characteristics. The first record is a file header containing the number of spectral channels to process (NCHANS) and the number of line-of-sight segments in LOSMODL.

Each specification for the sensor spectral response characteristics contains two header records followed by a table of the wavelength (in microns) and the associated spectral response. The first header record is an identifier for the spectral band, and the second header record contains the number of records in the spectral response table for that band. Up to 100 tabulated values can be provided for the spectral response function, and the wavelength values for the tabulation need not be uniformly spaced.

Appendix C

OAREJ Input Files

SYSS\$INPUT (VAX/VMS)

This file, which is generally defined as terminal input, contains two namelist specifications.

NAMELIST 'WEIGHTS'

NW = number of field-of-view solid angles (≤ 15);

FOVW = array of up to 15 field-of-view solid angles, in steradians, corresponding to the supplied spectral filters.

NAMELIST 'READIN2'

ALTNEW = altitude of sensor (km);

NZEN = number of zenith angles or tangent heights for the sensor lines-of-sight (≤ 15);

ZENITH = array of up to 15 zenith angles for the sensor lines-of-sight (degrees);

TANHT = array of up to 15 tangent heights for the sensor lines-of-sight (km).

Note: Either ZENITH or TANHT values may be provided, but not both.

OARCURV

This file contains a sequence of namelist entries defining the offaxis rejection function in terms of rejection factors R for each sensor polar angle PHI and azimuthal angle THETA.

NAMELIST 'REJCURV'

PHI = polar angle for a line-of-sight with respect to the sensor axis (degrees);

THETA = array of up to 10 azimuthal angles about the sensor axis, corresponding to the single polar angle PHI (degrees);

R = array of up to 10 rejection factors, corresponding to each azimuthal angle THETA for the specified polar angle PHI.

The sequence must contain the same number of (THETA, R) pairs for each namelist entry, and is terminated by a negative value for PHI. The PHI values must appear in increasing order, and the THETA values for each namelist entry must appear in increasing order. Up to 120 'REJCURV' entries (120 PHI values) may be provided.

LOSFLT

This file contains a table of radiance model parameters, including the zenith angle, tangent height, and associated in-band atmospheric radiance for 25 lines-of-sight. Each record contains the following values (see also the LOWTRAN4 specification in Appendix A):

M	= model specification;
IHAZE	= aerosol specification;
ITYPE	= line-of-sight path;
V1	= lower frequency for LOWTRAN;
V2	= upper frequency for LOWTRAN;
DV	= frequency increment for LOWTRAN;
FLO	= lower frequency for sensor spectral filter;
FHI	= upper frequency for sensor spectral filter;
H1	= assumed sensor altitude for LOWTRAN;
BETAP	= zenith angle for line-of-sight;
HMIN	= tangent height for line-of-sight;
RAD	= in-band radiance for line-of-sight.

Each line-of-sight set for a single spectral band is preceded by a single header record identifying the spectral band, so there are 26 records associated with each spectral band.

Appendix D

OAREJ Output Files

OFFAXRD

The standard format of the OAREJ offaxis radiance tabulation file OFFAXRD is:

Altitude

Band-1 header

Zenith-1, In-band radiance-1, In-band flux-1

Zenith-2, In-band radiance-2, In-band flux-2

Zenith-3, In-band radiance-3, In-band flux-3

.

.

.

Zenith-K, In-band radiance-K, In-band flux-K

Band-2 header

Zenith-1, In-band radiance-1, In-band flux-1

Zenith-2, In-band radiance-2, In-band flux-2

Zenith-3, In-band radiance-3, In-band flux-3

.

.

.

Zenith-K, In-band radiance-K, In-band flux-K

.

.

.

Band-N header

Zenith-1, In-band radiance-1, In-band flux-1

Zenith-2, In-band radiance-2, In-band flux-2

Zenith-3, In-band radiance-3, In-band flux-3

.

.

.

Zenith-K, In-band radiance-K, In-band flux-K

where $K \leq 15$ and $N \leq 15$.

SIGMAPA

The file SIGMAPA contains the results of the azimuthal integrations for each polar angle in

OARCURV, to allow evaluation of the particular polar angles at which the offaxis radiance is most significant. The format of this file is:

Band-1 header, Zenith-1

1, Phi-1, Phi integrand-1, Theta integral-1

2, Phi-2, Phi integrand-2, Theta integral-2

3, Phi-3, Phi integrand-3, Theta integral-3

.

.

.

M, Phi-M, Phi integrand-M, Theta integral-M

Band-1 header, Zenith-2

1, Phi-1, Phi integrand-1, Theta integral-1

2, Phi-2, Phi integrand-2, Theta integral-2

3, Phi-3, Phi integrand-3, Theta integral-3

.

.

.

M, Phi-M, Phi integrand-M, Theta integral-M

.

.

.

Band-N header, Zenith-K

1, Phi-1, Phi integrand-1, Theta integral-1

2, Phi-2, Phi integrand-2, Theta integral-2

3, Phi-3, Phi integrand-3, Theta integral-3

.

.

.

M, Phi-M, Phi integrand-M, Theta integral-M

with $M \leq 120$, $K \leq 15$, and $N \leq 15$. The "Theta integral" is the azimuthal integral of atmospheric in-band radiance times offaxis rejection factor for a given sensor polar angle "phi", while the "Phi integrand" also includes the sine weighting factor for the sensor polar angle.

LOSRAD

The file LOSRAD contains a summary of the LOSFILT data used for the offaxis radiance calculations, listing the revised zenith angles corresponding to the original line-of-sight tangent height and the requested sensor altitude, and the associated in-band radiance value for each line-of-sight.

References

1. Atmospheric Transmittance/Radiance: Computer Code LOWTRAN 4, J.E.A. Selby, F.X. Kneizys, J.H. Chetwynd, Jr., and R.A. McClatchey, AFGL-TR-78-0053, 28-February-1978, ADA058643
2. Infrared Measurements of Zodiacal Light, T.L. Murdock and S.D. Price, The Astronomical Journal, Vol. 90, No. 2, February 1985.
3. Private communication, M. Anapol, April 1987.